



A 3D Z-Scheme Heterojunction Photocatalyst: Flower-Like Ag/AgBr/ $\text{Zn}_3\text{V}_2\text{O}_7(\text{OH})_2 \cdot 2\text{H}_2\text{O}$ and its Enhanced Visible-Light Photocatalytic Activities

Xiaoshuo Hou¹ · Ming Yang¹ · Hui Yu¹ · Ying Yang¹ · Dan Li¹ · Xiangting Dong¹

Received: 31 October 2020 / Accepted: 6 July 2021 / Published online: 15 September 2021
© The Minerals, Metals & Materials Society 2021

Abstract

In this work, a 3D Z-scheme photocatalyst Ag/AgBr/ $\text{Zn}_3\text{V}_2\text{O}_7(\text{OH})_2 \cdot 2\text{H}_2\text{O}$ (Ag/AgBr/ZVO) was synthesized by a hydrothermal method, and a subsequent surface deposition-optical reduction technique. The prepared flower-like Ag/AgBr/ZVO was characterized by scanning electron microscopy (SEM), x-ray powder diffraction (XRD), x-ray photoelectron spectroscopy (XPS), UV-vis spectrophotometry, N_2 adsorption-desorption isotherm based on Brunauer-Emmett-Teller (BET) theory, and electrochemical tests. The photocatalytic degradation performance of the catalyst was investigated by the degradation of methylene blue (MB) dye by visible light irradiation. Compared with bare $\text{Zn}_3\text{V}_2\text{O}_7(\text{OH})_2 \cdot 2\text{H}_2\text{O}$ (ZVO) nanoflowers, the photocatalytic effect of the 3D Z-scheme heterojunction Ag/AgBr/ZVO was significantly enhanced. The catalyst of 2h-Ag/AgBr/ZVO exhibited the strongest photocatalytic activity, of which the MB degradation rate is about 98.8% in 100 min, which was about five times that of pure ZVO. The increase in the photodegradation rate is ascribed to the accelerated interface charge-transfer process, the faster photogenerated carrier separation rate and the enhancement of visible light absorption. In view of the trapping of the reaction intermediate and the electron spin resonance (ESR) measurement, we propose a possible Z-scheme photocatalytic mechanism. This improved visible-light response likely originates from a synergistic effect of the different components. This work offered an ideal method for producing stable, efficient, and recyclable photocatalysts suitable for use in the visible light range.

Keywords Z-scheme · hydrothermal method · photocatalytic mechanism · Ag/AgBr/ $\text{Zn}_3\text{V}_2\text{O}_7(\text{OH})_2 \cdot 2\text{H}_2\text{O}$

Introduction

Over the past several decades, industry and the economy have rapidly developed, and humans' living environment and quality have gradually deteriorated. We are facing a huge energy crisis and environmental pollution while enjoying and consuming precious resources from nature.^{1–4} Photocatalysis has gradually attracted the interest of many

researchers due to its cost-effective and green applications in environmental protection.⁵ As we all know, the photodegradation process involves light excitation, the separation and migration processes of the photogenerated charges carriers, and finally the redox reaction of organic molecules.⁶

On Earth, vanadium is a diffusely distributed transition element. As important functional inorganic materials, transition metal vanadium oxide and vanadate materials have long been studied due to their rich structural chemistry and excellent kinetics.^{7,8} The diversity of vanadium oxidation states from +2 to +5 affords many unique compounds and coordination numbers. They have numerous applications in optical devices,⁹ electrode materials for lithium batteries,^{10,11} catalysts^{12,13} magnetic materials,^{14,15} gas sensors,¹⁶ and electrochemical capacitors.^{17–19} In contrast to the tendency of vanadium oxides to become amorphous, a second metal is introduced and arranged between the vanadium oxide layers to form columns that stabilize the framework of vanadium oxides. A lot of research have been conducted

✉ Ming Yang
minnie_yang@163.com

✉ Hui Yu
yh2001101@163.com

✉ Xiangting Dong
dongxiangting888@sohu.com

¹ School of Chemistry and Environmental Engineering,
Changchun University of Science and Technology,
Changchun 130022, People's Republic of China

on the synthesis and properties of various structured-metal vanadates, such as $\text{Na}_{1.1}\text{V}_3\text{O}_{7.9}$,²⁰ BiVO_4 nanoparticles,²¹ FeVO_4 nanorods,²² $\text{Li}_{0.04}\text{V}_2\text{O}_5$ nanowires²³ and $\text{Zn}_3\text{V}_3\text{O}_8$ nanoflowers.²⁴

According to previous theoretical studies, the V 3d orbital has a lower conduction band position. It can be deduced that a semiconductor material containing vanadium element may have a more suitable energy band structure, and may be a good photocatalyst raw material. Some examples include BiVO_4 ,²⁵ $\text{Zn}_2\text{V}_2\text{O}_7$,²⁶ and $\text{Zn}_3(\text{VO}_4)_2$.¹² Among metal vanadate photocatalysts, $\text{Zn}_3\text{V}_2\text{O}_7(\text{OH})_2 \cdot 2\text{H}_2\text{O}$ was a particularly important semiconductor photocatalyst material.^{27–29} This is due to its special crystal structure and suitable energy level positions. Hexagonal-phase ZVO is a frame structure composed of a Zn-O tetrahedron layer and a V-O octahedron layer that are mutually bonded in an alternative fashion.³⁰ In addition, there were channels for electrons and holes to move between the V-O layers. It was easier for photogenerated carriers to migrate to the catalyst surface for redox reactions. However, due to the wide band gap of ZVO and weaker absorption of visible light, its application in photocatalysis has been limited. For example, Wang *et al.* prepared ZVO nanoplates, and discovered that the ZVO had photocatalytic degradation performance towards methylene blue (MB) under UV light irradiation.²⁹ Modification of ZVO is an effective means of making up for this deficiency. Zhan *et al.* designed a $\text{g-C}_3\text{N}_4/\text{Zn}_3\text{V}_2\text{O}_7(\text{OH})_2(\text{H}_2\text{O})_2$ with high photocatalytic activities,³⁰ of which the absorption range under visible light was significantly expanded. Therefore, so as to improve the absorption range of ZVO under visible light, we needed to find a narrow band gap semiconductor to modify it.

AgBr was a representative photosensitive semiconductor ($E_g = 2.6 \text{ eV}$).³¹ Thereby, AgBr was widely employed to decorate photocatalysts to boost photocatalytic performance. When AgBr was exposed to light, the Ag^+ in it are easily reduced to Ag due to its photosensitivity. As far as we know, some noble metals (Au or Ag) possess a surface plasmon resonance (SPR) effect that can greatly enhance the width of the absorption bands.^{32,33} Noble metal-semiconductor composite materials, as heterojunction photocatalysts containing two kinds of visible light response photocatalyst components with visible light response and precious metals with surface plasmon resonance, are considered as ideal means to degrade pollutants.^{34,35} Until now, more and more attention has been paid to Ag/AgX ($X = \text{Br}, \text{Cl}, \text{I}$) because these structures are effective at degrading harmful chemicals in visible light.^{36–38} A series of Ag@AgX ($X = \text{Cl}, \text{Br}, \text{I}$) plasmonic photocatalysts were synthesized by Wang and his co-workers, in which Ag⁰ reduced from Ag⁺ of AgX was supposed to prompt optical absorption in the visible light region.³⁹ Cai *et al.* devised Ag/AgCl photocatalysts, and the optical absorption of the

as-prepared photocatalysts was significantly enhanced, which was ascribed to the enhanced optical absorption due to the Ag⁰.⁴⁰ However, the silver halide species (AgX, $X = \text{Br}$ or Cl) always suffers from decomposition under sunlight irradiation, resulting in its poor performance in the photocatalytic reaction and thus reducing the stability and efficiency of the catalyst. Additionally, silver nanoparticles produced by silver halide are mostly large and disordered, which adversely impacts the photocatalytic activity. In this case, we chose ZVO nanoflowers as the support material, because it was not only a visible-light-driven photocatalyst but also has a large surface area, making it an ideal candidate. Ag⁰ could also be employed as an electron mediator in Z-scheme photocatalysts. Many researchers have discovered a large number of Z-scheme semiconductor composites with Ag/AgBr, such as $\text{CeO}_2\text{-Ag/AgBr}$,⁴¹ AgI/Ag/AgBr ,⁴² $\text{Ag-AgBr@Bi}_{20}\text{TiO}_{32}$,⁴³ and $\text{Ag@AgBr/g-C}_3\text{N}_4$.⁴⁴ Owing to retaining the superior reduction ability of the conduction band (CB) and the superior oxidation ability of the valence band (VB), the Z-scheme system exhibited higher photocatalytic performance than the single photocatalyst.⁴¹ Anchoring Ag/AgBr on the surface of ZVO seemed to be an ideal choice for raising the photocatalytic degradation rate of ZVO.

In this paper, we successfully synthesized ZVO with flower-like nanostructures through a template-free hydrothermal route, which has weaker photocatalytic activity under visible light. However, because ZVO has a large forbidden band width, its absorption range of visible light is narrow. Therefore, we modified it with a narrow band gap semiconductor AgBr. By depositing Ag/AgBr on the flower-shaped sphere ZVO, a 3D Ag/AgBr/ZVO Z-type heterojunction photocatalyst was cleverly constructed. Cetyltrimethylammonium bromide (CTAB) was chosen as both of surfactant and Br source. Through the reaction of AgNO_3 with CTAB in ZVO aqueous solution, some AgBr nanoparticles are deposited on the ZVO. The obtained AgBr/ZVO was then irradiated under the xenon lamp to obtain the Ag/AgBr/ZVO. The formation of the Ag/AgBr/ZVO heterojunction was confirmed by scanning electron microscopy (SEM), x-ray photoelectron spectroscopy (XPS) and Mott-Schottky measurement. The photocatalytic degradation performance of Ag/AgBr/ZVO was estimated by the photodegradation of MB under visible light irradiation. The results demonstrated that the photocatalytic ability of the 2 h-Ag/AgBr/ZVO was remarkably boosted as compared with bare ZVO. What's more, success in preparing the 3D hetero-nanostructure Ag/AgBr/ZVO was a significant milestone to creating some new types of 3D hetero-nanostructure functional materials. However, our study was only performed in the laboratory stage and has not been used in practical applications.

Experimental Section

Reagents and Chemicals

Zinc nitrate hexahydrate ($\text{Zn}(\text{NO}_3)_2 \cdot 6\text{H}_2\text{O}$) and ammonium metavanadate (NH_4VO_3) were purchased from Aladdin Reagent Co. Ltd., China. CTAB was received from Shenyang Reagent Factory. Silver nitrate (AgNO_3) was received from Beijing Chemical Plant, China. Deionized water and ethanol were used for washing and dissolution during the experiment.

Synthesis of ZVO Nanomaterials

NH_4VO_3 and $\text{Zn}(\text{NO}_3)_2 \cdot 6\text{H}_2\text{O}$ (3:2 molar ratio) was dissolved into 40 mL deionized water. The obtained solution was diverted into a 50 mL autoclave to perform a hydrothermal treatment at 120°C for 3 h, 6 h, 12 h, 18 h. The precipitates were collected by filtration, and washed with deionized water and ethanol. Finally, the precipitates were dried at 60°C.

Synthesis of Ag/AgBr/ZVO Heterostructures

We selected flower-like ZVO as the support for Ag/AgBr. 30 mg of ZVO powder obtained above was dispersed in 20 mL CTAB aqueous solution (0.01 mol/L) with magnetic stirring for 1 h. Then, 10 mL of silver nitrate solution (0.01 mol/L) was added dropwise, and the resulting mixed liquid was placed in a dark environment and stirred for 1 h. After stirring for 1 h, the mixture was then irradiated under sunlight for about X (X = 1,2,3,4) h to obtain X h-Ag/AgBr/ZVO. The color of the product changed from white to light gray, indicating that silver nanoparticles were formed. The product was filtered, washed with deionized water, and dried in air at 60°C to obtain the powder sample. For comparison, the same method was used to synthesize AgBr/ $\text{Zn}_3\text{V}_2\text{O}_7(\text{OH})_2 \cdot 2\text{H}_2\text{O}$ (AgBr/ZVO) without visible light irradiation.

Characterization

X-ray diffraction (XRD) patterns were collected on a Siemens D5005 diffractometer using Cu-K α radiation ($\lambda = 1.5418 \text{ \AA}$ and operating at 30 kV and 20 mA). SEM images were assumed on a JEOL JSM-5600L instrument. Physical adsorption of nitrogen was performed on a Micromeritics ASAP2010 M volumetric adsorption analyzer at 77 K. A sample was degassed in vacuum at 573 K for 12 h before measurement. Surface area was calculated based on the Brunauer-Emmett-Teller (BET) model, while pore size was

computed using the Barret-Joyner-Halenda (BJH) method. The UV-vis diffuse reflectance spectra (UV-vis DRS) were measured using a UV-vis spectrophotometer (UV-vis 2550, Shimadzu, Japan). XPS (AXIS) ULTRA, Japan) characterizations were performed on a photoelectron spectrometer with a monochromatized Al K α x-ray source. Excitation was used to investigate the distribution of Zn, V, Ag, Br and O in the Ag/AgBr/ZVO composite material.

Photocatalytic Activity Measurements

Photocatalysis was evaluated through the photodegradation of MB under a xenon lamp source (Microsolar300, Beijing Perfectlight, light intensity 200 mW/cm², $\lambda \geq 420 \text{ nm}$). In a typical reaction, 50 mg photocatalyst (ZVO, AgBr/ZVO, 1 h-Ag/AgBr/ZVO, 2 h-Ag/AgBr/ZVO, 3 h-Ag/AgBr/ZVO, 4 h-Ag/AgBr/ZVO) was placed in 100 mL MB aqueous solution (5 mg/L). A 4 mL solution sample was taken at 20 min intervals during the experiment.

The degradation rate was calculated using Eq. (1), where C_0 and C_t were the initial and residual pollutant concentration before and after visible-light irradiation, respectively. The first-order kinetic equation (Eq. (2)) was used to fit the experimental data, where k was the reaction rate constant, and t was the reaction time.

$$\text{Degradation rate} = (C_0 - C_t)/C_t \times 100\% \quad (1)$$

$$\ln(C_t/C_0) = k \times t \quad (2)$$

Results and Discussion

Structure and Morphology Characterization of Catalysts

The synthetic process of ZVO and 3D Z-scheme heterojunction photocatalyst Ag/AgBr/ZVO was depicted in Fig. 1. Hexagonal-phase ZVO is a frame structure composed of a Zn-O tetrahedron layer and a V-O octahedron layer alternately bonded to each other, therefore, ZVO crystallizes easily to form a nanosheet structure. When the reaction time was 3 h, ZVO nanosheets self-assembled to form a 3D flower-like structure. We selected flower-like ZVO as the skeleton for Ag/AgBr, and a 3D Z-scheme heterojunction photocatalyst Ag/AgBr/ZVO was prepared by subsequent surface deposition and photoreduction technology. When the reaction time increases, the flower-like morphology of ZVO was destroyed, and the nanobelts were grown from broken nanoflowers, which demonstrated that the hydrothermal time was a key factor in the morphology of ZVO.²⁷ We can infer this conclusion from the XRD and SEM results.

Fig. 1 Schematic illustration of the synthesis of ZVO and photocatalyst Ag/AgBr/ZVO.

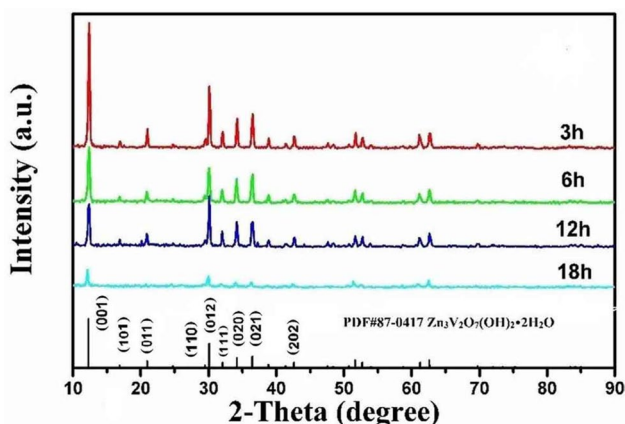
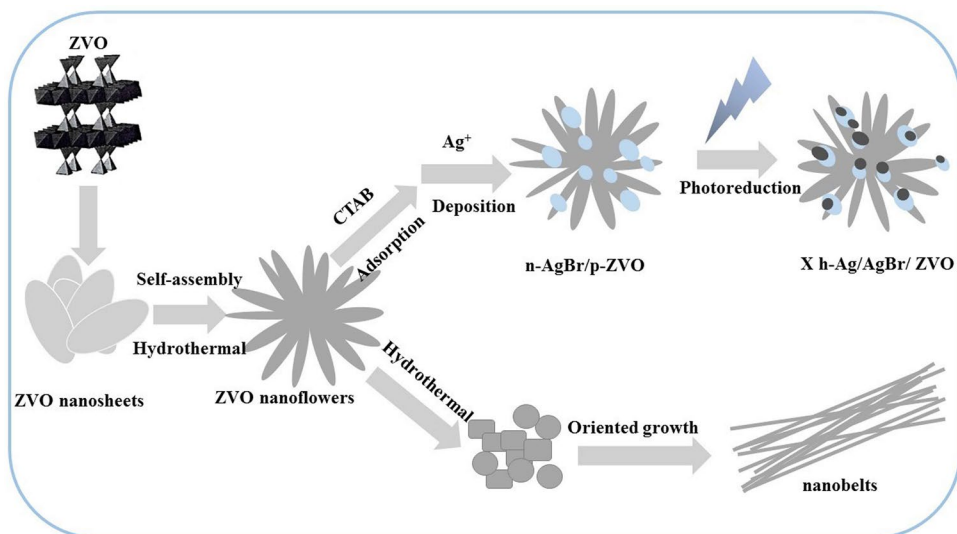


Fig. 2 XRD patterns for ZVO nanostructures obtained at 120°C for different reaction time.

Figure 2 shows the XRD patterns of all the as-synthesized ZVO. All of the samples show a single phase, and no secondary phase is observed. The main diffraction peaks of 12.29°, 30.10°, 34.19°, 36.46°, respectively correspond to the diffraction of the (001), (012), (020) and (021) planes of ZVO (PDF# 87-0417). Strong and sharp peaks suggested that the product was well crystallized. When the reaction time increases, the intensity of the (001) diffraction peak decreases gradually and the intensity is minimized at 18 h of reaction time, indicating the growth direction of samples was altered. Compared with those previous studies of ZVO synthesized using NaVO_3 instead of NH_4VO_3 as a vanadium source,^{30,45} we concluded that the NH_4^+ cations play a key role in determining the crystal growth orientation along either the [110] or [001] axis.⁴⁶

The crystal structures and phases of $\text{Zn}_3\text{V}_2\text{O}_7(\text{OH})_2 \cdot 2\text{H}_2\text{O}$, AgBr, and X h-Ag/AgBr/ZVO (X = 1, 2, 3, 4) were detected via XRD patterns. As shown in Fig. 3, after the introduction

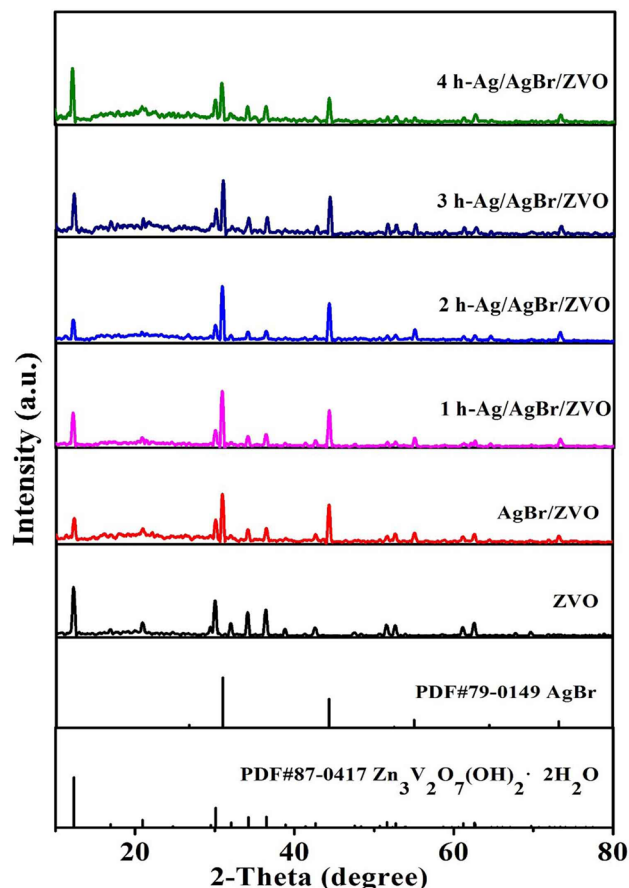


Fig. 3 XRD patterns of samples.

of silver bromide and silver, the structure of ZVO has not changed, suggesting that the introduced nanoparticles may not be incorporated into the crystal lattice of ZVO. Compared with bare ZVO, three new peaks at 31.0°, 44.2° and

72.2 ° appeared, which could be assigned to face-centered cubic AgBr (PDF#79-0149).⁴⁷ Because the Ag⁰ amounts were low and the weak peaks were covered by the background, its diffraction peaks were not observed

SEM images of the ZVO are shown in Fig. 4a–d. It can be seen that the reaction time was a key factor in changing the morphology. Figure 4 shows that with increasing reaction time, the morphology of the products changes from a nanoflower (Fig. 4a) to a nanobelt (Fig. 4d). A large number of sphere-like nanoflowers are distributed evenly, indicating that a significant proportion (above 90 %) of the products presents a uniform sphere-like nanoflower structure. The average diameter of the nanoflowers was approximately 4–5 μm. The individual ZVO ‘flower’ still consisted of a large quantity of homogeneous nanosheets. The nanobelts are several to tens of micrometers in length and 200–300 nm in width.

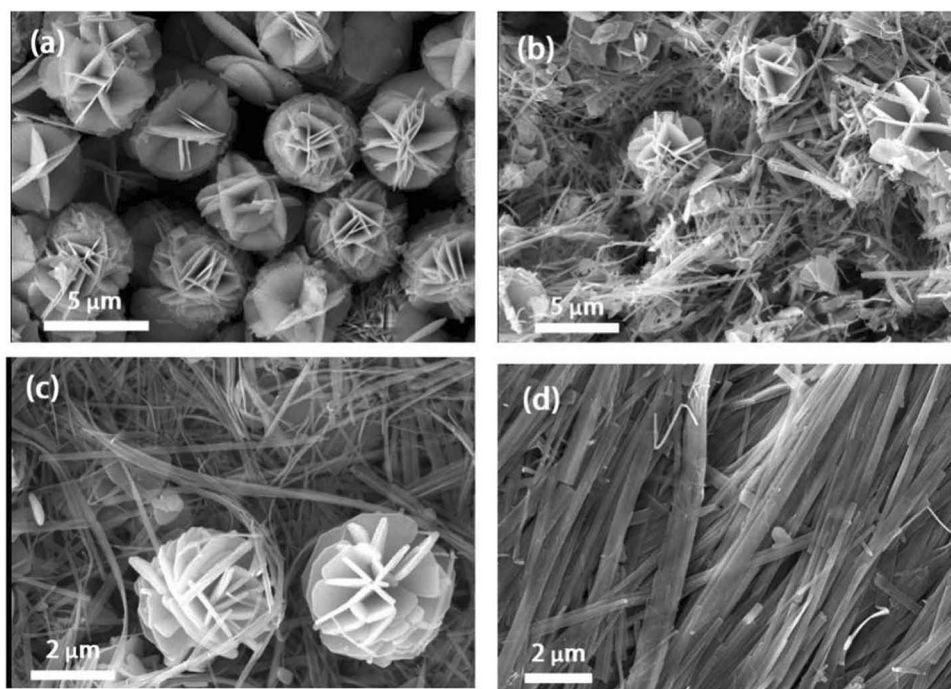
The morphologies of ZVO, AgBr/ ZVO and X h-Ag/AgBr/ZVO (X=1, 2, 3, 4 h) were further investigated through SEM images as shown in Fig. 5. From Fig. 5a and the illustration, it can be seen that bare ZVO products exhibited a regular flower-like morphology, and has perfect uniformity and dispersibility. Compared to the bare ZVO, the surfaces of AgBr/ZVO (Fig. 5b) become rough and some AgBr nanoparticles are gathered on the ZVO nanoflowers. From Fig. 5c–e, it was found that the flower-like morphology remains intact after growth of Ag/AgBr particles on the surface of ZVO. As the photoreduction time changes, the size of the Ag/AgBr nanoparticles also changed significantly. The presence of ZVO prevents

the polymerization of the Ag/AgBr nanoparticles, which increases the specific surface area and active sites of the catalyst to a certain extent. A large amount of Ag/AgBr nanoparticles could effectively increase the absorbance of the catalyst. Figure 5f represents the morphology of 4 h-Ag/AgBr/ZVO. The morphology of ZVO was slightly destroyed, and Ag/AgBr nanoparticles gathered on the ZVO surface. This was unfavorable for the photocatalytic process.

The element mapping images of 2 h-Ag/AgBr/ZVO are exhibited in Fig. 6. Figure 6a–f demonstrates that Ag and Br are uniformly distributed on the surface of the ZVO, and Ag, Br, V, Zn, and O are also uniformly dispersed in the composites. This indicates that the corresponding composite catalysts were prepared successfully.

The surface elemental compositions and chemical states of the 2 h-Ag/AgBr/ZVO sample were analyzed by XPS. The survey XPS spectrum (Fig. 7a) shows that the Ag/AgBr/ZVO sample contained V, Zn, O, Br, and Ag. As displayed in Fig. 7b, two peaks located at 516.64 eV and 524.32 eV were attributed to V 2p_{3/2} and V 2p_{1/2}, respectively, corresponding to V⁵⁺ in Zn₃V₂O₇(OH)₂·2H₂O. Figure 7c shows the Zn 2p XPS spectrum. Two individual peaks located at 1022.7 eV and 1045.6 eV were attributed to Zn 2p_{3/2} and Zn 2p_{1/2}, respectively. Figure 7d shows that the apparent characteristic peak at 530.4 eV²⁶ was assigned to the O 1s binding energy. Two characteristic peaks located at 67.7 eV (Br 3d_{5/2}) and 68.7 eV (Br 3d_{3/2}) in Fig. 7e indicate the existence of Br⁻ in the AgBr structure.⁴⁸ In Fig. 7f, the peaks located at 373.6 and 367.5 eV

Fig. 4 SEM images of as-obtained ZVO nanostructures at 120°C for different reaction times: (a) 3 h, (b) 6 h, (c) 12 h, (d) 18 h.



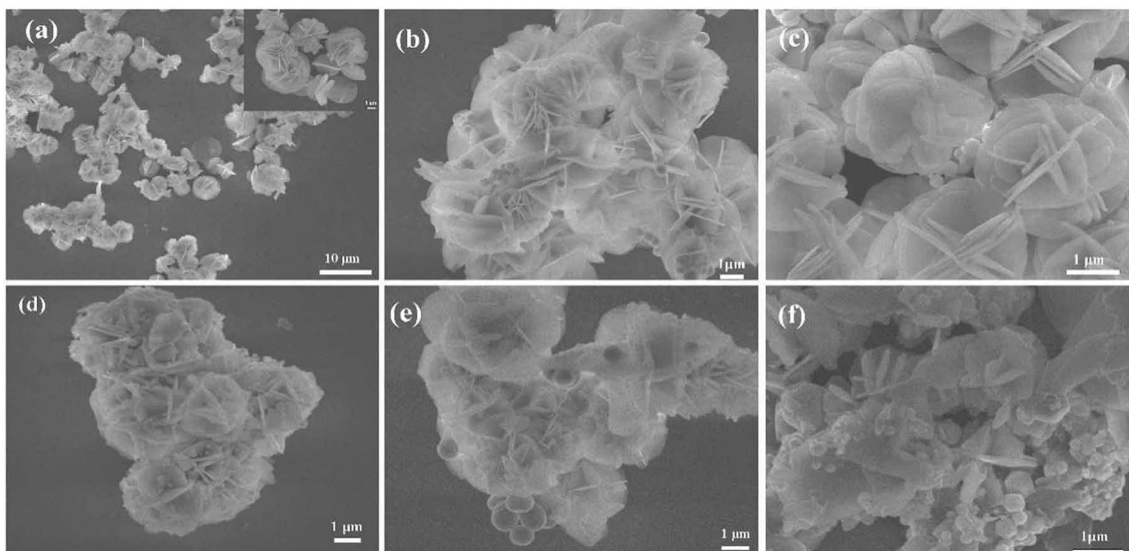


Fig. 5 SEM images of (a) ZVO, (b) AgBr/ZVO, (c) 1 h-Ag/AgBr/ZVO, (d) 2 h-Ag/AgBr/ZVO, (e) 3 h-Ag/AgBr/ZVO, (f) 4 h-Ag/AgBr/ZVO.

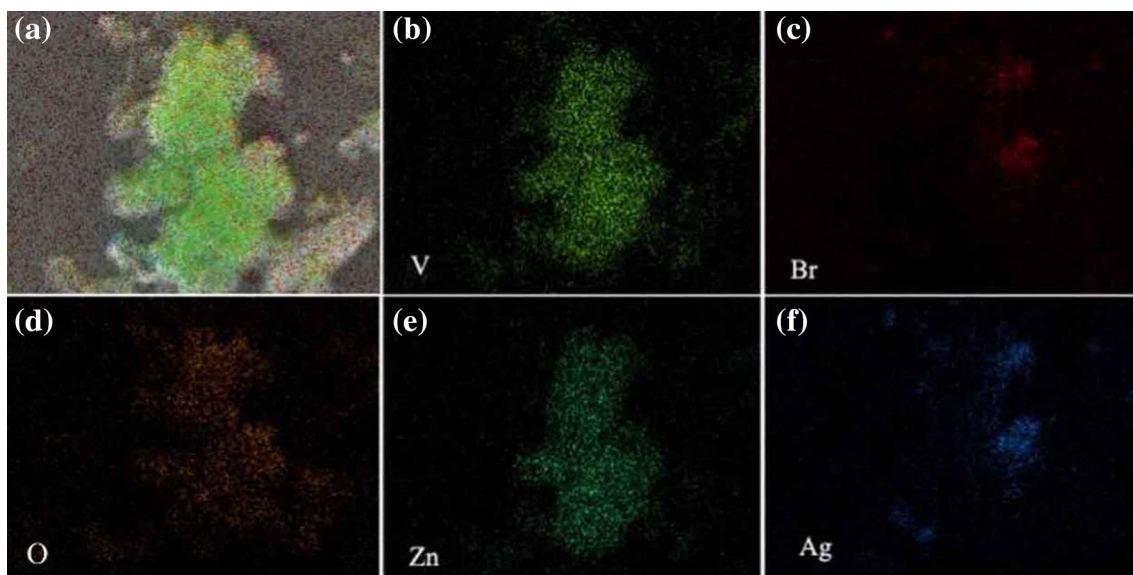


Fig. 6 The SEM image (a) and element distribution images of (b) V, (c) Br, (d) O, (e) Zn and (f) Ag in 2h-Ag/AgBr/ZVO.

were attributed to the Ag $3d_{3/2}$ and Ag $3d_{5/2}$ of Ag^+ , and the peaks at 374.1 and 368.1 eV belong to the Ag $3d_{3/2}$ and Ag $3d_{5/2}$ of Ag^0 .⁴⁹

The specific surface area of the catalyst has a certain effect on its photocatalytic performance. Research showed that the photocatalytic activity of the photocatalysts is positively related to their specific surface area. As shown in Fig. 8, the isothermal adsorption-desorption curve of the 2 h-Ag/AgBr/ZVO showed a IV-type isotherm with a H1 hysteresis loop. The specific surface area of the 2 h-Ag/AgBr/ZVO determined by the BET method was $39.56 \text{ m}^2 \text{ g}^{-1}$. The

pore sizes were determined by the BJH method. The pore size of the 2 h-Ag/AgBr/ZVO sample was 3.4 nm.

Photocatalytic Properties

The UV-vis DRS was used to characterize the optical properties of the catalyst. As shown in Fig. 9 a, the maximum absorption edge of bare ZVO was around 405 nm, which showed the ZVO has a corresponding effect in the near visible light region. The maximum absorption edge of AgBr/ZVO was unchanged compared with ZVO. In contrast to

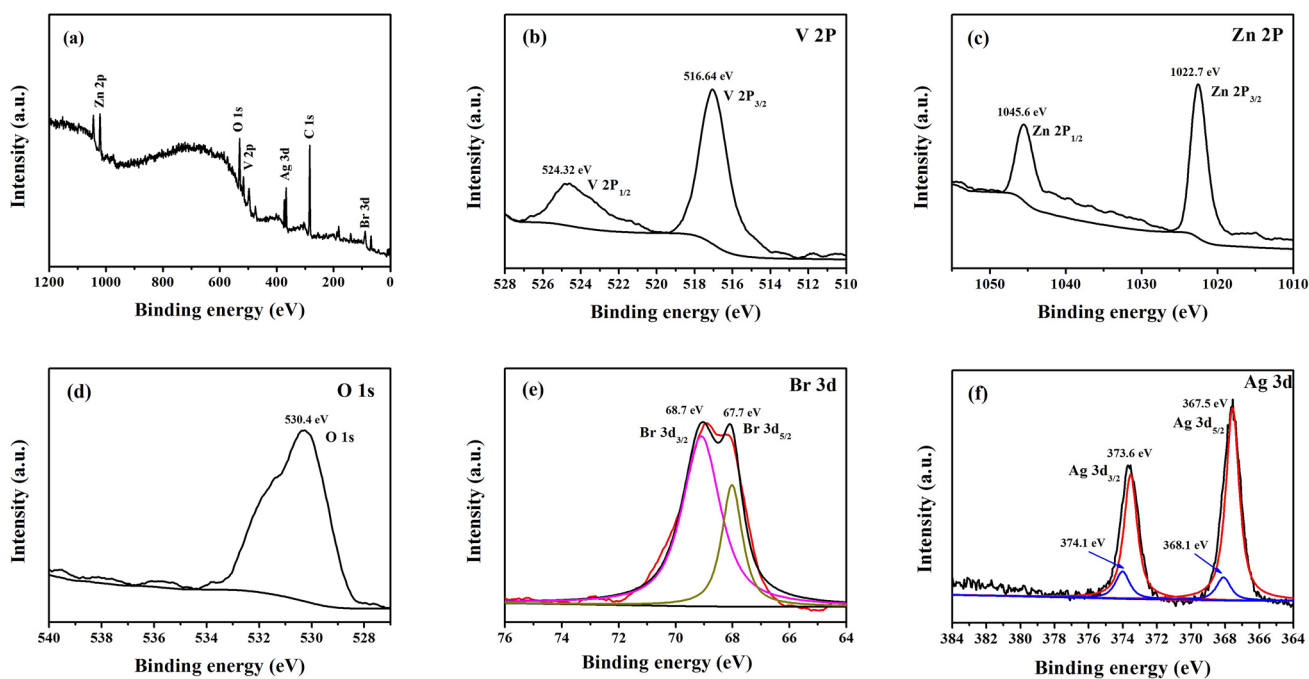


Fig. 7 XPS spectra of 2 h-Ag/AgBr/ZVO. (a) Survey spectra, (b) V 2p, (c) Zn 2p, (d) O 1s, (e) Br 3d, (f) Ag 3d.

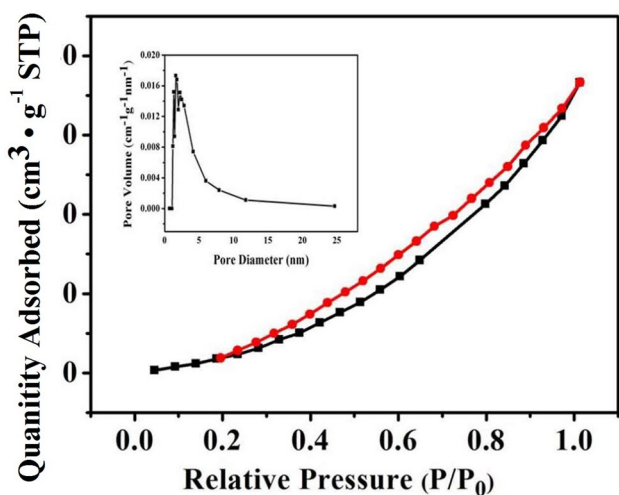


Fig. 8 Nitrogen adsorption-desorption isotherms and pore-size distribution curve of 2 h-Ag/AgBr/ZVO.

ZVO and AgBr/ZVO, the absorption edges of X h-Ag/AgBr/ZVO photocatalysts showed a significant red shift. This showed that the band gap of the composite materials become smaller. The absorption wavelengths were the biggest when the illumination time was 2 h. The band gap energy (E_g) could be evaluated by the Kubelka–Munk method.⁵⁰ As shown in Fig. 9b, the E_g values for bare ZVO and 2 h-Ag/AgBr/ZVO are 3.06 and 2.71 eV, respectively. The results confirmed that there is a red shift in the 2 h-Ag/

AgBr/ZVO sample compared with the bare ZVO. As shown in Fig. 9c, the photocatalysis efficiency of as-prepared X h-Ag/AgBr/ZVO ($x = 1, 2, 3,$ and 4), AgBr/ZVO and bare ZVO catalysts were examined by degrading MB under visible light. The MB degradation rate of ZVO was 19.8 % after irradiation for 100 min, while the photocatalytic degradation rate of MB by AgBr/ZVO reached 78 %. However the photodegradation rate of ternary X h-Ag/AgBr/ZVO photocatalysts were significantly improved in comparison with bare ZVO and AgBr/ZVO. Among those samples, the 2 h-Ag/AgBr/ZVO photocatalyst had the fastest photodegradation rate, and 98.8 % of MB was degraded in 100 min. under visible light illumination, while 89.1, 84, and 80 % of MB were degraded over 1 h - Ag/AgBr/ZVO, 3 h-Ag/AgBr/ZVO and 4 h-Ag/AgBr/ZVO, respectively. Figure 9d displays the pseudo-first-order kinetic curves of MB degradation over as-prepared catalysts. The reaction constant k value of MB degradation over 2 h-Ag/AgBr/ZVO was the highest, being about 0.042, which was about 21 times and 2.7 times that of ZVO and AgBr/ZVO. This indicated that the photocatalytic ability of ZVO can be effectively enhanced through compositing with Ag and AgBr.

Photocatalytic Mechanism

Additionally, as one of the most effective methods for depicting the charge transfer and separation efficiency, electrochemical impedance spectroscopy (EIS) of as-prepared catalysts were employed. From Fig. 10a, ZVO possesses

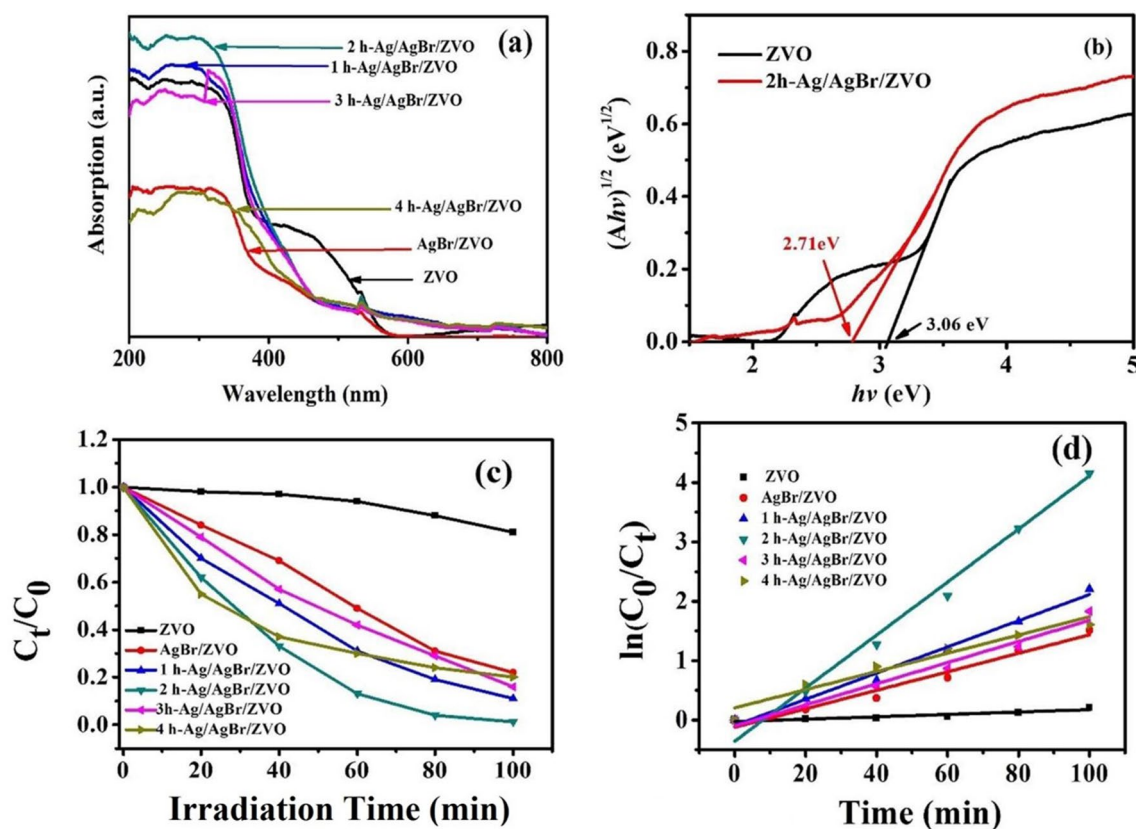


Fig. 9 (a) UV-vis DRS of the samples, (b) the corresponding band gap estimation based on the Kubelka–Munk theory, (c) elimination of MB over photocatalysts, (d) the first-order kinetics of MB photocatalytic degradation.

the maximum radius of the Nyquist plot. The introduction of Ag/AgBr nanoparticles into ZVO caused an apparent decline in the arc radius of the Nyquist plot, revealing that the Ag/AgBr/ZVO composites had the smallest interface transfer resistance. However, the semicircular radius of X h-Ag/AgBr/ZVO ($X = 1, 3, 4$ h) were larger than that of 2 h-Ag/AgBr/ZVO, indicating that the photogenerated carriers could be separated faster in 2 h-Ag/AgBr/ZVO, because the Ag/AgBr promotes the construction of an effective heterostructure between the interfaces of ZVO and AgBr. The appropriate light exposure time was also a key factor in the preparation of excellent performance photocatalysts. Figure 10b depicts the Tafel analysis, in which 2 h-Ag/AgBr/ZVO exhibits the largest anodic Tafel slope as compared with ZVO and X h-Ag/AgBr/ZVO ($X = 1, 3, 4$). The larger anodic Tafel slope shows that 2 h-Ag/AgBr/ZVO has higher reactivity and better electrochemical performance. The ZVO and AgBr were employed in M-S measurements. Normally, in an M-S curve, a positive slope represents an n-type semiconductor, whereas a negative slope represents a p-type semiconductor. Obviously, bare ZVO is a typical p-type semiconductor (Fig. 10c), and bare AgBr is a typical n type semiconductor (Fig. 10d). We could also observe that the E_{fb}

of ZVO and AgBr were 1.02 and -0.14 eV, respectively. For the most n (p)-type semiconductors, the CB (VB) position was believed to be about 0.1 eV above (below) the E_{fb} .⁵¹ The E_{VB} of ZVO was 1.12 eV (vs. Ag/AgCl), and this value can be further transformed to the normal hydrogen electrode (NHE) by the Nernst equation (Eq. (3)).⁵² The VB of ZVO is 1.317 eV (vs. NHE), and the CB was -1.743 eV. According to the band gap of AgBr (2.6 eV),³² the VB and CB of AgBr are 2.557 eV and -0.043 eV, respectively.

$$E_{NHE} = E_{Ag/AgCl} + 0.197 \quad (3)$$

During the process of the photocatalytic reaction, some main active substances would be produced, among which $\bullet O_2^-$, $\bullet OH$ and h^+ are the three most important active groups. $Na_2C_2O_4$, BQ and IPA were used as scavenging agents for h^+ , $\bullet O_2^-$ and $\bullet OH$, respectively. We performed trapping experiments of active species to determine that the substituent groups played a role. As shown in Fig. 11a, when $Na_2C_2O_4$, BQ and IPA were added separately, the degradation rate of MB decreased from 98.8 to 53.8 % (IPA), 62.6 % ($Na_2C_2O_4$) and 75 % (BQ) within 100 min, respectively.

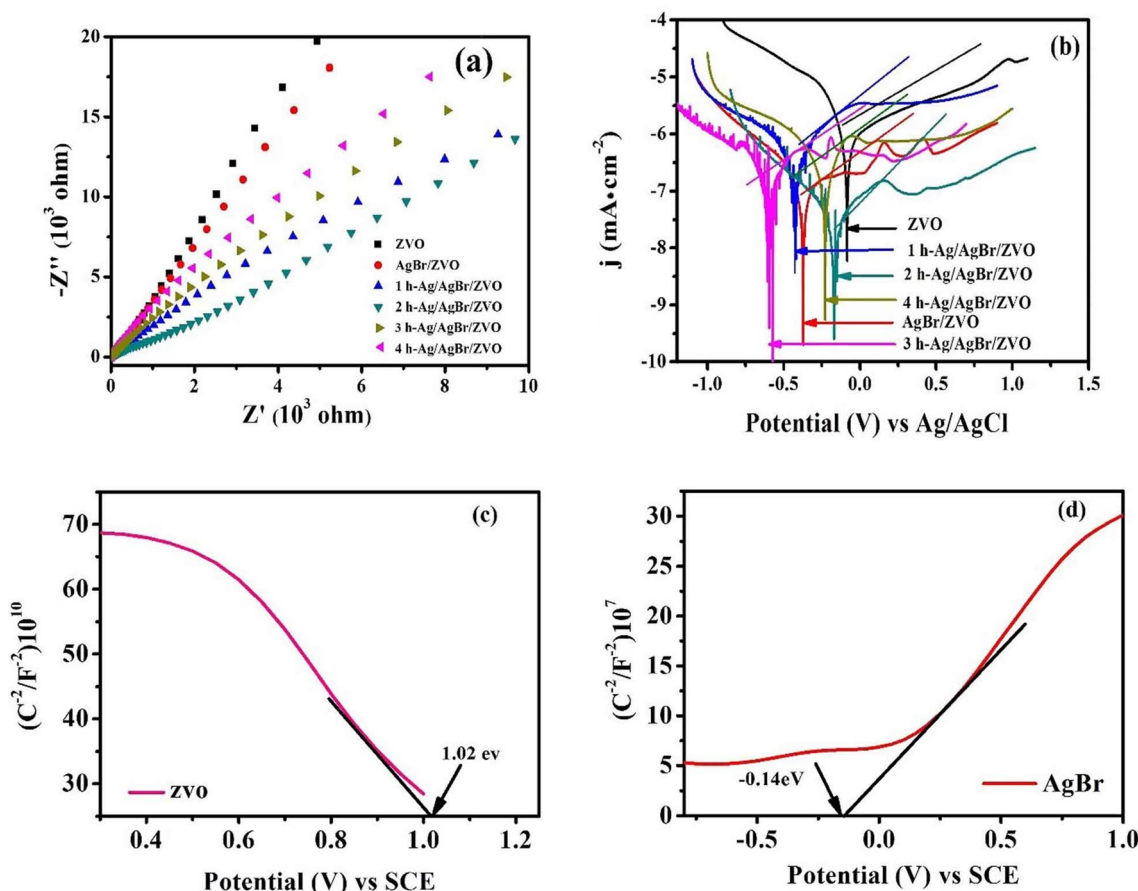
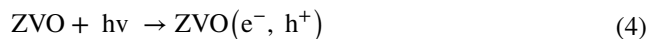


Fig 10 (a) EIS spectra and (b) Tafel polarization curves (c) and (d) Mott-Schottky plots of ZVO and AgBr in 0.1 M Na_2SO_4 aqueous solution (pH = 7).

Thence, the $\bullet\text{O}_2^-$, h^+ and $\bullet\text{OH}$ are the main active group in the photocatalytic reaction. From Fig. 11 c and d, the signals of $\bullet\text{O}_2^-$ and $\bullet\text{OH}$ cannot be detected under dark conditions. However, the signals of $\bullet\text{O}_2^-$ and $\bullet\text{OH}$ appeared under visible light irradiation. This corresponded to the trapping experiment results.

As we all know, the electron (e^-) and hole (h^+) separation ability as well as the light absorption ability of the catalyst are the key factors that determine its photocatalytic ability. Based on all the observations, we posed a possible photocatalytic mechanism, illustrated in Fig. 12. As shown in Fig. 12a, according to the energy band position of the AgBr and ZVO, a conventional heterojunction can be formed between AgBr and ZVO. When visible light was irradiated on the catalyst surface, both AgBr and ZVO could be stimulated. Because the CB position and VB position of ZVO was higher than AgBr, the e^- on the CB of ZVO flow to the CB of AgBr, and the h^+ on the VB of AgBr flow to the VB of ZVO, rapidly separating e^-/h^+ . However the CB (0.043 eV vs. NHE) of AgBr was lower than the potential of $\text{O}_2/\bullet\text{O}_2^-$ (-0.046 eV vs. NHE), the e^- obtained on the CB of

AgBr will reduce Ag^+ to Ag^0 , causing photo-corrosion of AgBr. Furthermore, the h^+ remaining at the VB potential of ZVO (1.317 eV vs. NHE) do not have enough capacity to oxidize water into hydroxyl radicals, owing to their potential being lower than the $\text{H}_2\text{O}/\bullet\text{OH}$ potential (2.37 eV vs. NHE).⁴¹ Based on this, we proposed a Z-scheme system, in which Ag nanoparticles act as a bridge between e^-/h^+ . In Fig. 12b, when exposed to visible light, the e^- on the CB of AgBr flow to the Ag nanoparticles, and integrate with the h^+ transferred from the VB of ZVO. It accelerates the separation of e^-/h^+ , and improves the stability of the composite. The e^- on the CB of ZVO reacted with the adsorbed oxygen on the surface of the ZVO to generate superoxide radicals, and the h^+ on the VB of AgBr reacted with water to generate hydroxyl radicals. This analysis was identical to the results of the ESR and the trapping of reactive species. The specific reflection process was as follows:



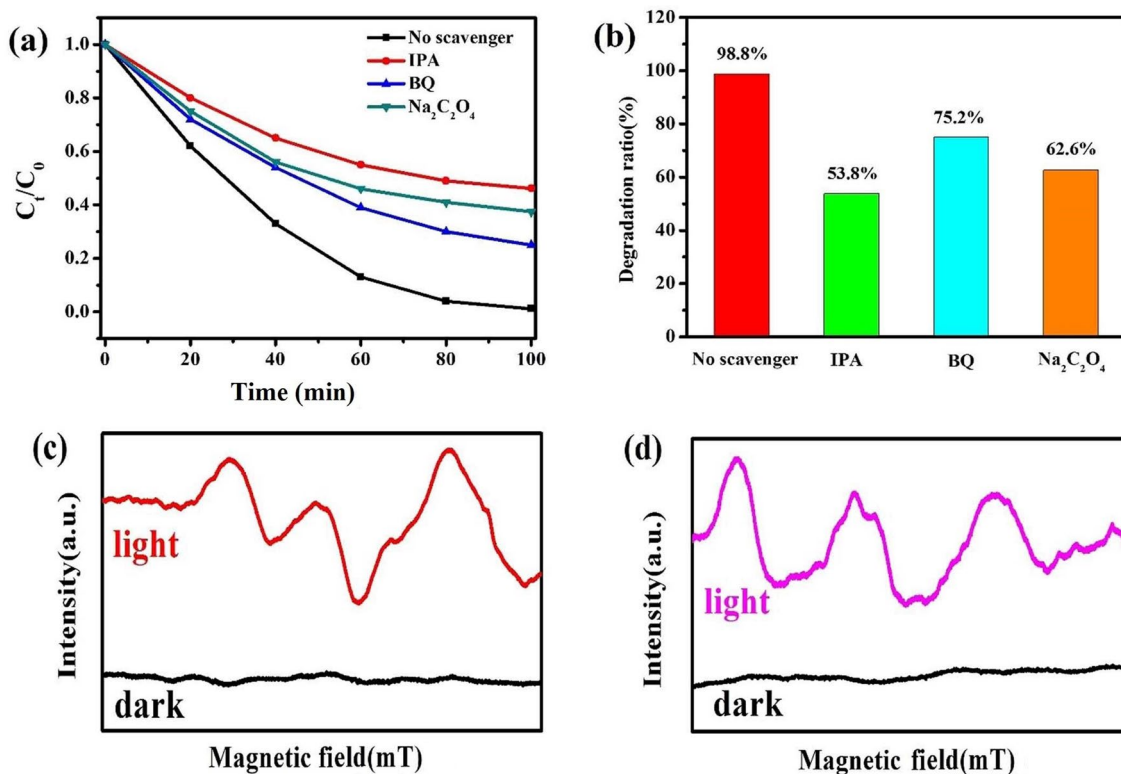


Fig. 11 (a) Photo-degradation of MB under visible light irradiation with scavengers of IPA, BQ and $Na_2C_2O_4$ over 2 h-Ag/AgBr/ZVO; (b) degradation values of the 2 h-Ag/AgBr/ZVO after the addition of

a trapping agent; DMPO spin-trapping ESR spectra for 2 h-Ag/AgBr/ZVO; (c) in methanol dispersion for DMPO $\bullet O_2^-$ and (d) in aqueous dispersion for DMPO $\bullet OH$.

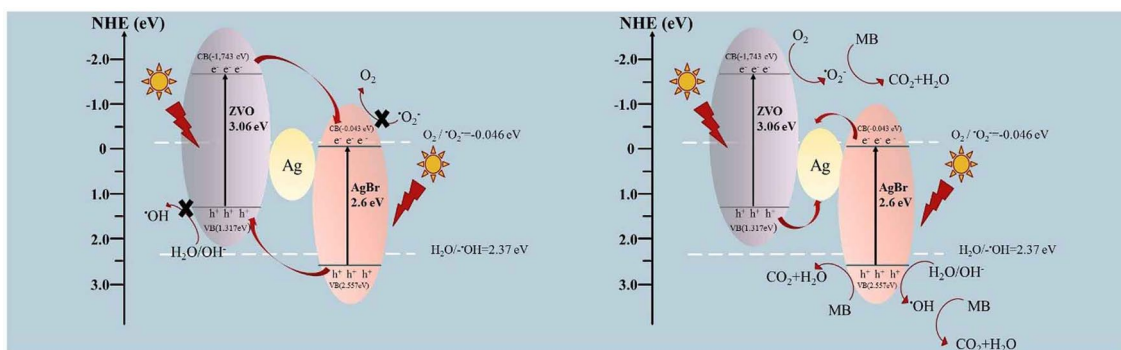
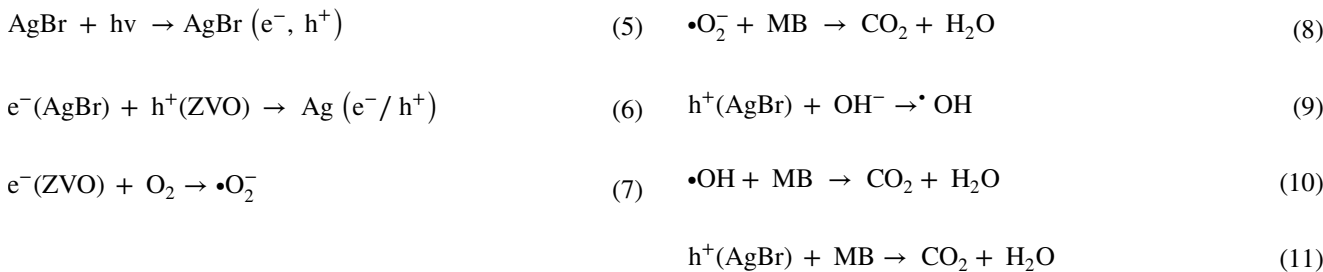


Fig. 12 Possible reaction mechanism for Ag/AgBr/ZVO (a) the conventional heterojunction; (b) the Z-scheme heterojunction.



Conclusions

To summarize, we prepared ZVO with different morphologies by a hydrothermal method. We selected flower-shaped ZVO as a support for Ag/AgBr. A 3D Z-scheme heterojunction was constructed by depositing AgBr on the surface, and a Z-scheme system Ag/AgBr/ZVO was successfully prepared through a subsequent photoreduction route. The size of the 3D flower-like Ag/AgBr/ZVO composite particle was about 2.5 μm . The specific surface area of the 2 h-Ag/AgBr/ZVO was 39.56 $\text{m}^2 \text{g}^{-1}$. The 2 h-Ag/AgBr/ZVO has a narrower band gap (2.71 eV). The prepared photocatalyst had a fast degradation rate towards MB under visible light irradiation. The photoreduction time was key factor during photodegradation. The catalyst 2h-Ag/AgBr/ZVO exhibited the strongest photocatalytic activity, of which the MB degradation efficiency is about 98.8 % in 100 min. and the reaction constant k values of MB degradation over 2 h-Ag/AgBr/ZVO was 0.042. EIS and Tafel measurements indicated that the composite photocatalyst has a higher electron-hole separation efficiency. Active species trapping experiments and ESR confirmed that h^+ , $\bullet\text{OH}$, and $\bullet\text{O}_2^-$ were the main active groups involved in photodegradation of MB. According to the band position of the ZVO and AgBr and identified active species, we speculated that the photocatalysis mechanism over Ag/AgBr/ZVO composites was a Z-scheme.

Acknowledgment We were very grateful for the support of the work by the National Natural Science Foundation of China (No. 51572034, 51802027), the Science and Technology Development Planning Project of Jilin Province (No. 20200201534JC, 20190103035JH).

Declarations

Conflict of interest The authors declare that they have no conflict of interest.

References

- O. Miarov, A. Tal, and D. Avisar, *J. Environ. Manag.* 254, 109794 (2020).
- H.J. Gao, X.X. Zhao, H.M. Zhang, J.F. Chen, S.F. Wang, and H. Yang, *J. Electron. Mater.* 49, 5248 (2020).
- Y.L. Gou, S.C. Yang, Y.J. Cheng, Y. Song, P.W. Qiao, P.Z. Li, and J.S. Ma, *Chem. Eng. J.* 356, 524 (2019).
- R.Q. Guan, H.J. Zhai, D.W. Sun, J.K. Zhang, Y. Wang, and J.X. Li, *Chem. Res. Chin. Univ.* 35, 271 (2019).
- M.X. Ran, H. Wang, W. Cui, J.Y. Li, P. Chen, Y.J. Sun, J.P. Sheng, Y. Zhou, Y.X. Zhang, F. Dong, and A.C.S. Appl. Mater. Interfaces. 11, 47984 (2019).
- H. Zhao, C. Tian, J. Mei, S.J. Yang, and P.K. Weng, *Chem. Eng. J.* 390, 124551 (2020).
- K. Fan, H.Y. Zou, L.L. Duan, and L.C. Sun, *Adv. Energy Mater.* 10, 1903571 (2019).
- M.H. Khorasanizadeh, R. Monsef, O. Amiri, M. Amiri, and M. Salavati-Niasari, *Ultrason. Sonochem.* 58, 104686 (2019).
- B. Etemadi, J. Mazloom, and F.E. Ghodsi, *Mater. Sci. Semicond. Process.* 61, 99 (2017).
- R. Chen, Z.Q. Wang, Z.X. Chen, P.J. Wang, G.Z. Fang, J. Zhou, X.P. Tan, and S.Q. Liang, *J. Alloys Compd.* 772, 852 (2019).
- K. Hua, X.J. Li, Z.W. Fu, D. Fang, R. Bao, J.H. Yi, and Z.P. Luo, *J. Solid State Chem.* 273, 287 (2019).
- R.M. Kakhki, and F. Ahsani, *J. Mater. Sci-Mater El.* 29, 3767 (2017).
- C. Zhuang, L.Q. Tang, Z.T. Yu, T.X. Peng, Y.C. Zhang, L. Li, Y. Zhou, and Z.G. Zou, *Catal. Sci. Technol.* 9, 182 (2019).
- R. Li, Y. Xiao, S.H. Wang, X.M. Jiang, Y.Y. Tang, J.G. Xu, Y. Yan, F.K. Zheng, and G.C. Guo, *J. Mater. Chem. C.* 5, 513 (2017).
- D. Zhou, R. Takahashi, Y.Y. Zhou, D. Kim, V.K. Suresh, Y.H. Chu, Q. He, P. Munroe, M. Lippmaa, J. Seidel, and N. Valanoor, *Adv Electron Mater.* 3, 1600295 (2017).
- K. Hua, M.M. Cui, Z.P. Luo, D. Fang, R. Bao, Q. Qi, J.H. Yi, B.S. Sun, and C.C. Chen, *J. Alloys Compd.* 801, 581 (2019).
- H.A. Ghaly, A.G. El-Deen, E.R. Souaya, and N.K. Allam, *Electrochim. Acta.* 310, 58 (2019).
- A. Mishra, G. Bera, P. Mal, G. Padmaja, P. Sen, P. Das, B. Chakraborty, and G.R. Turpu, *Appl. Surf. Sci.* 488, 221 (2019).
- H.W. Liu, and Y.P. Cui, *Mater. Lett.* 228, 369 (2018).
- B.H. She, L.T. Shan, H.J. Chen, J. Zhou, X. Gun, G.Z. Fang, X.X. Cao, and S.Q. Liang, *J. Energy Chem.* 37, 172 (2019).
- C. Regmi, Y.K. Kshetri, D. Dhakal, J.K. Sohng, F. Rosei, and S.W. Lee, *Appl. Surf. Sci.* 466, 787 (2019).
- H.X. Chen, J. Zeng, M.D. Chen, Z.G. Chen, M.X. Ji, J.Z. Zhao, J.X. Xia, and H.M. Li, *Chin. J. Catal.* 40, 744 (2019).
- K. Hua, X.J. Li, D. Fang, J.H. Yi, R. Bao, and Z.P. Luo, *Appl. Surf. Sci.* 447, 610 (2018).
- P. Liu, J.H. Yi, R. Bao, and D. Fang, *New J. Chem.* 43, 7482 (2019).
- Z.L. Li, C.Y. Jin, M. Wang, J. Kang, Z.M. Wu, D.E. Yang, and T. Zhu, *Sep. Purif. Technol.* 232, 115937 (2020).
- C.L. Yu, D.B. Zeng, F.Y. Chen, H.B. Ji, J.L. Zeng, D.B. Li, and K. Yang, *Appl. Catal. A.* 578, 70 (2019).
- R. Shi, Y.J. Wang, F. Zhou, and Y.F. Zhu, *J. Mater. Chem.* 21, 6313 (2011).
- L.L. Yang, Y.W. Tang, L.P. Tong, H. Zhou, J. Ding, T.X. Fan, and D. Zhang, *Appl. Surf. Sci.* 346, 115 (2015).
- F.F. Wang, W.B. Wu, X.J. Sun, S.Y. Song, Y. Xing, J.W. Wang, D.H. Yu, and Z.M. Su, *Mater. Charact.* 86, 139 (2013).
- S. Zhan, F. Zhou, N.B. Huang, Y.F. Yin, M. Wang, Y.F. Yang, and Y.J. Liu, *J. Mol. Catal. A: Chem.* 401, 41 (2015).
- Y. He, R. H. Yuan, K. H. Leung M, *Mater. Lett.* 236, 394(2019)
- Y. Zeng, N. Guo, X.J. Xu, Y. Yu, Q.Y. Wang, N. Wang, X.R. Han, and H.W. Yu, *Chemosphere* 227, 589 (2019).
- C. Liang, H. Guo, L. Zhang, M. Ruan, C.G. Niu, H.P. Feng, X.J. Wen, N. Tang, H.Y. Liu, and G.M. Zeng, *Chem. Eng. J.* 372, 12 (2019).
- W. Li, Q. Ma, X. Wang, S.A. He, M. Li, and L.F. Ren, *Appl. Surf. Sci.* 494, 275 (2019).
- S.T. Guan, R.S. Li, X.F. Sun, T. Xian, and H. Yang, *Mater. Technol.* (2020). <https://doi.org/10.1080/10667857.2020.1782062>.
- Z.G. Jia, Q.H. Chen, C.Y. Li, Z.Y. Li, D.Q. Zhang, R. Chu, and L. Wu, *J. Phys. Chem. Solids.* 140, 109360 (2020).
- D.K. Bhatt, and U.D. Patel, *J. Phys. Chem. Solids.* 135, 109118 (2019).
- Y. Sang, L. Kuai, C. Chen, Z. Fang, and B. Geng, *ACS Appl. Mater. Interfaces.* 6, 5061 (2014).
- Y.N. Wang, H.P. Liu, B. Wu, T.Y. Zhou, J.M. Wang, J. Zhou, S. Li, F. Cao, and G.W. Qin, *J. Alloys Compd.* 776, 948 (2019).
- B. Cai, J. Wang, S.Y. Gan, D.X. Han, Z.J. Wu, and L. Niu, *J. Mater. Chem. A.* 2, 5280 (2014).

41. X.J. Wen, C.G. Niu, L. Zhang, C. Liang, H. Guo, and G.M. Zeng, *J. Catal.* 358, 141 (2018).
42. H.L. Lin, J. Cao, B.D. Luo, B.Y. Xu, and S.F. Chen, *Catal. Commun.* 21, 91 (2012).
43. R.Y. Xie, L.P. Zhang, H. Xu, Y. Zhong, X.F. Sui, and Z.P. Mao, *J. Mol. Catal. A: Chem.* 406, 194 (2015).
44. Y.X. Yang, W. Guo, Y.N. Guo, Y.H. Zhao, X. Yuan, and Y.H. Guo, *J. Hazard. Mater.* 271, 150 (2014).
45. A. Bayat, A.R. Mahjoub, and M.M. Amini, *J Mater Sci-Mater El.* 29, 2915 (2018).
46. J. Zhu, S.L. Wang, S.H. Xie, and H.X. Li, *Chem. Commun.* 47, 4403 (2011).
47. J. Zhang, J. Wang, H.H. Xu, X.Z. Lv, Y.X. Zeng, J.Z. Duan, and B.R. Hou, *RSC Adv.* 9, 37109 (2019).
48. W. Li, X. Wang, M. Li, S.A. He, Q. Ma, and X. Wang, *Appl. Catal. B: Environ.* 268, 118384 (2020).
49. P. Yu, X.Q. Zhou, Z.F. Li, and Y.C. Yan, *Sci. Total. Environ.* 705, 135639 (2020).
50. S. P. Tandon, and J. P. Gupta, *phys Status Solidi B.* 38, 363(2006)
51. S.M. Sun, W.Z. Wang, D.Z. Li, L. Zhang, and D. Jiang, *ACS Catal.* 4, 3498 (2014).
52. H. Guo, C. Niu, D.W. Huang, N. Tang, C. Liang, L. Zhang, X.J. Wen, Y. Yang, W.J. Wang, and G.M. Zeng, *Chem. Eng. J.* 360, 349 (2019).

Publisher's Note Springer Nature remains neutral with regard to jurisdictional claims in published maps and institutional affiliations.